JASA ARTICLE

Method for measuring acoustic radiation force of a focused ultrasound beam acting on an elastic sphere[a)]

Liubov M. Kotelnikova,[1] Sergey A. Tsysar,[1] Dmitry A. Nikolaev,[1] and Oleg A. Sapozhnikov[1,2,b)]

[1]*Faculty of Physics, Moscow State University, Leninskie Gory, Moscow, 119991, Russia*

[2]*Center for Industrial and Medical Ultrasound, Applied Physics Laboratory, University of Washington, 1013 NE 40th Street, Seattle, WA 98105, USA*

ABSTRACT:

Acoustic radiation force (ARF) is a nonlinear phenomenon resulting from the wave momentum transfer to an absorbing or scattering target. ARF allows objects to be remotely manipulated, pushed, trapped, or pulled, which is used in medical applications such as kidney stone expulsion or acoustic tweezers. Such applications require development of methods for precision ARF measurements and calculations. The purpose of this paper is to present a method for direct measurement of the axial component of the ARF exerted by an ultrasound beam on its axis acting on a millimeter-sized spherical particle in a liquid. The method consists of weighing a rigid frame with a scatterer on electronic scales, similar to the radiation force balance method of measuring the total acoustic beam power. The capabilities of the method are demonstrated by applying it to spheres of different diameters (2–8 mm) and compositions (steel, glass). The additional objective is to provide experimental validation of the theoretical model of Sapozhnikov and Bailey [J. Acoust. Soc. Am. **133**, (2013)], previously developed to calculate the ARF of an arbitrary acoustic beam on an elastic sphere in a liquid or gaseous medium based on the angular spectrum approach.

© *2025 Acoustical Society of America*. https://doi.org/10.1121/10.0035939

(Received 7 August 2024; revised 25 December 2024; accepted 2 February 2025; published online 21 February 2025)

[Editor: Philip L. Marston] Pages: 1391–1402

I. INTRODUCTION

The phenomenon of acoustic radiation force (ARF) has been studied for many decades.[1] One of the strongest drivers of this development is the wide range of biomedical applications, such as the capture and manipulation of small particles, cells and larger objects (acoustic tweezers), acoustic levitation, elastography, biofabrication of tissue spheroid constructs, and more.[2–5] There is a rapidly developing field related to the expulsion and directional movement of kidney stones and their fragments in the human body using focused ultrasound.[6–9] Because of the evolving research in remote object manipulation, a quantitative study is of interest to investigate the ability of megahertz ultrasound to exert force on millimeter-sized scatterers. This requires the development of methods to calculate the ARF acting on objects of any shape and composition in different acoustic beams and accurately measure the force of small magnitude.

To date, various theoretical models have been developed to calculate the ARF acting on different scatterers in different media. Some works are limited to the case of plane wave analysis or absolutely rigid or soft scatterers.[10,11] In Ref. 12, a spherical object is analyzed in a soft elastic medium. Approximate models are also used.[13] The present study considers the situation of an arbitrary acoustic beam in liquid falling on a spherical scatterer whose dimensions are comparable to, or larger than, the wavelength. For this case, Sapozhnikov and Bailey have derived analytical expressions for calculating the ARF acting on a sphere using the angular spectrum method (marked below as the SB model), which is convenient for calculating the radiation force based on the acoustic hologram.[14] An alternative approach using the spherical coordinate system has also been suggested for this case.[15] As shown in Ref. 16, these approaches lead to the same results.

Despite the large number of theoretical models proposed, the number of experimental papers providing verification is much smaller. The majority of experiments described in the literature concerning the measurement of ARF magnitude acting on spherical scatterers in liquid were based on the determination of the angle of deflection of a sphere suspended on a thread from its equilibrium position.[17–22] Although these techniques are effective in measuring force accurately, they have a number of disadvantages due to the displacement of the sphere from its original position. The measurement results remain largely unaffected by a change in spatial location if the structure of the acoustic field is similar to that of a plane wave. However, for focused ultrasound beams, where the focal beam waist can be as small as 1 mm or less, strong field inhomogeneity leads to a correspondingly pronounced ARF inhomogeneity. Under these conditions, small changes in the position of the scatterer during force measurements result in the inability to accurately determine the position of the sphere in the field, making force measurement along any predefined axis a challenge.

[a)]The basic concept of this article and preliminary results have previously been published by O. Sapozhnikov, L. M. Kotelnikova, D. A. Nikolaev, and S. A. Tsysar [Proc. Mtgs. Acoust. **48**(1), 045005 (2022)].

[b)]Email: oleg@acs366.phys.msu.ru

Some experimental techniques have previously been proposed for the ARF measurement in liquid for beams with complex structures. For example, a method has been developed to measure the transverse (lateral) ARF component of the vortex beam by positioning a sphere on a flat platform attached to a rotational stage.[23] The force magnitude was determined from the maximum angle of rotation of the platform at which the sphere was held stationary by counterbalancing forces acting on it. The accuracy of this method was 10%–20%. To measure the axial component of the ARF exerted by a focused beam on a millimeter-sized spherical scatterer, a method has been suggested based on the balance between the ARF, gravity, and buoyancy forces during the levitation of the particle under study.[24,25] The numerical and experimental results were found to agree within 10% in the post-focal and pre-focal regions. Force oscillations were observed in the focal region due to the occurrence of standing waves between the scatterer and the transducer surface. Despite positive results, the process of implementing this method was quite labor-intensive and time-consuming. To calibrate the axial stiffness of a single-beam acoustic tweezers, an experimental method for measuring the axial component of the radiation force acting on millimeter spheres in air was investigated.[26] The method consisted of observing the axial oscillations of a trapped bead in a microgravity environment and estimating the ARF value from their frequency. The experimental results showed a systematic overestimation of the theoretical model by a factor of about 2 due to experimental uncertainties (20%–30%) and theoretical model assumptions. Thus, existing methods allow the magnitude of the radiation force acting on a sphere to be estimated, but are difficult to use and not very accurate.

The current paper describes a new method for the direct measurement of the axial component of the acoustic radiation force exerted by an ultrasound beam on its axis acting on a millimeter-sized elastic sphere in a liquid. The sphere is fixed in a system of thin fishing lines attached to a rigid frame that surrounds the tank walls without touching them and rests on an electronic balance. By weighing the frame with the scatterer, the value of the vertical component of the radiation force is determined. The preliminary results obtained with this method have previously been published.[27] The purpose of this paper is to demonstrate the validity of the proposed method as well as to validate the theoretical approach for calculation of the radiation force of an arbitrary acoustic beam on an elastic sphere in liquid based on the angular spectrum approach (SB model).

II. MATERIALS AND METHODS

A. Theoretical model

1. *ARF of an arbitrary beam on an elastic sphere*

The analytical expressions obtained in the SB model were used for the numerical calculation of the ARF. A brief description is given below.

Consider a monochromatic acoustic beam directed along the z axis falling on an isotropic elastic sphere of radius a immersed in an ideal fluid. Cartesian (x, y, z) and spherical (r, θ, φ) coordinate systems are introduced, the origin of the coordinate systems is set at the center of the sphere, and the angle $\theta = 0°$ corresponds to the direction of the z axis, $z = r\cos\theta$. The ARF exerted by the beam on the scatterer has three Cartesian components: $\mathbf{F}_{rad} = (F_x, F_y, F_z)$. Each component of the force depends on three spatial coordinates (x, y, z): The force acting on the scatterer will vary in magnitude and direction if the scatterer is placed at different points in the field. The lateral components (F_x and F_y) when the sphere is placed on the beam axis are small in a beam that is close to axisymmetric. The axial (vertical) component considered in this paper is defined by the following expression:

$$F_z = -\frac{1}{4\pi^2 \rho c^2 k^2} \mathrm{Re}\left\{ \sum_{n=0}^{\infty} \Psi_n \sum_{m=-n}^{n} B_{nm} H_{nm} H^*_{n+1,m} \right\}. \quad (1)$$

Here, c is the speed of sound in the immersion fluid (water), ρ is the density of the fluid, $k = \omega/c = 2\pi f/c$ is the wave number, f is the frequency, $\mathrm{Re}[\cdot]$ indicates the real part of the term in brackets, the asterisk denotes a complex conjugate,

$$B_{nm} = \sqrt{\frac{(n+m+1)(n-m+1)}{(2n+1)(2n+3)}} \quad (2)$$

are the known numerical coefficients, and

$$\Psi_n = (1 + 2c_n)\left(1 + 2c^*_{n+1}\right) - 1 \quad (3)$$

are coefficients determined by the elastic properties of the scatterer and the surrounding medium. Auxiliary coefficients are

$$c_n = -\frac{\Gamma_n j_n(ka) - ka\, j_n'(ka)}{\Gamma_n h_n^{(1)}(ka) - ka\, h_n^{(1)'}(ka)}, \quad (4)$$

where the primes indicate differentiation with respect to the argument, characterize the scattering and depend on the known properties of the fluid and the sphere material, namely, on the speed of sound c and the density ρ of the fluid, the density of the sphere material ρ_*, and the combinations $k_l a$, $k_t a$, where $k_l = \omega/c_l$, $k_t = \omega/c_t$, and c_l and c_t are the velocities of the longitudinal and transverse waves in the sphere. $h_n^{(1)}(\xi) = j_n(\xi) + i n_n(\xi)$ are spherical Hankel functions of the first kind, where $j_n(\xi)$ and $n_n(\xi)$ are spherical Bessel and Neumann functions, respectively. Coefficients

$$H_{nm} = \iint_{k_x^2 + k_y^2 \le k^2} dk_x dk_y S(k_x, k_y) Y^*_{nm}(\theta_k, \varphi_k) \quad (5)$$

fully specify the incident field with an angular spectrum $S(k_x, k_y)$, and $Y_{nm}(\theta, \varphi)$ are spherical harmonics. Expressions for full forms of coefficients Γ_n as well as the angles θ_k and φ_k are given in Ref. 14. The angular (spatial) spectrum of the beam is determined by the formula

$$S(k_x, k_y) = \int_{-\infty}^{+\infty}\int_{-\infty}^{+\infty} dx\, dy\, p(x,y) e^{-ik_x x - ik_y y}, \quad (6)$$

where $p(x, y)$ is the acoustic pressure complex amplitude of the harmonic wave of specified frequency f in the plane of the position of the center of the sphere.

For the analysis, it is convenient to introduce a dimensionless ARF.[25] In particular, the axial component of the dimensionless radiation force is calculated as follows:

$$Y_z = \frac{F_z c}{W}. \quad (7)$$

Here, W is the total acoustic beam power, which can be calculated from the angular spectrum of the beam:[14,28]

$$W = \frac{1}{8\pi^2 \rho c} \iint\limits_{k_x^2 + k_y^2 \le k^2} dk_x dk_y \left|S(k_x, k_y)\right|^2 \sqrt{1 - \frac{k_x^2 + k_y^2}{k^2}}. \quad (8)$$

2. Finding the angular spectrum of an acoustic beam

In order to numerically calculate the ARF exerted by a linear acoustic beam, it is essential to determine the spatial structure of the beam, specifically its angular spectrum. The field structure of the focusing source used in this study can be calculated using the Rayleigh integral, assuming that the amplitude of the normal component of the vibration velocity is uniform across its surface (piston model).[29] However, the actual nature of the surface vibration is non-uniform due to various factors, such as Lamb wave excitation in the piezoceramic plate rim[30] and design features of the plate mounting, making such a description only approximate. Therefore, a more accurate method is used in this study: measurement of the transient acoustic hologram of the source followed by processing using the standard method.[31,32]

3. Minimizing sound reflection from a piezoelectric transducer (PT)

When conducting measurements of the radiation force acting on a spherical scatterer from a focusing PT, standing waves are generated between the surfaces of the PT and the sphere due to multiple reflections of waves from these two surfaces. These standing waves become particularly significant when the sphere is within the focal area.[25] Similar oscillations have been studied in a number of papers by other authors.[33,34] To minimize their effect on the force measurements, the approach outlined in Ref. 35 was used to reduce the reflection coefficient from the PT surface by adjusting the electrical impedance of its load. Initially, the method was developed and experimentally tested for a setup with a large-diameter flat source and a flat reflector installed parallel to each other, producing the plane wave mode. Theoretical analysis has demonstrated that at frequencies where the imaginary part of the PT impedance vanishes (e.g., at the antiresonance frequency), it is possible to completely eliminate the sound reflection from the PT by using an electrical load with a purely active impedance equal to the impedance of the PT.

In this study, the aforementioned method is applied to minimize the coefficient of reflection from a concave PT with an air backing, which is used in ARF measurements. An elastic sphere placed at the focus of the source acts as a reflector. It can be assumed that the propagation, reflection, and re-reflection of spherical waves are analogous to those of plane waves in the one-dimensional case. Various resistances are considered as the electrical load of the PT to minimize the reflection coefficient in the vicinity of the antiresonance frequency.

B. Experimental arrangement

This section presents a precise method for measuring the ARF acting on finite-size millimeter scatterers. This method can be applied to scatterers of any shape (ellipsoids, cylinders, polyhedrons, etc.), but in this paper it is considered for elastic spheres. The source of sound waves can also be of any type.

1. Elastic targets

The characteristics of the targets are summarized in Table I. Steel (grade AISI 440-C stainless steel) and glass (sodium–calcium–silicate glass, i.e., crystal glass) spheres were used.

The diameters and masses of the spheres were measured using a micrometer with a 0.01 mm graduation and an electronic balance with an accuracy of 0.004 g. The deviation from sphericity did not exceed 10–20 μm. Knowledge of the mass and diameter of the sphere was used to calculate its density, ρ_*. The final density error was less than 5%. Varying the densities within this error did not affect the value of the ARF.

In addition to density, the magnitude of the radiation force also depends on the value of parameters characterizing the elastic properties of the scatterer material (longitudinal and shear wave velocities). The study of the ARF therefore requires a knowledge of these elastic properties as accurately as possible. Since the elastic constants of the scatterers of interest are not always known exactly, and their value varies according to the chemical composition and internal structure determined by manufacturing and processing methods, we have previously carried out research to determine the elastic parameters of spheres. They were determined from experimental measurements of the frequency dependence of the forward scattering amplitude.[36] The values obtained (c_l, c_t) are also listed in Table I. Errors in the determination of the longitudinal and shear wave velocities do not exceed 2% and 1%, respectively.

https://doi.org/10.1121/10.0035939

TABLE I. Geometric and elastic properties of spherical targets used in experiments. The errors in the determination of ρ_*, c_l, and c_t do not exceed 5%, 2%, and 1%, respectively.

Sample name	Material	Diameter (mm)	Density ρ_* (kg/m^3)	Longitudinal velocity, c_l (m/s)[a]	Shear velocity, c_t (m/s)[a]
S2.8	Steel	2.77	7480	5930	3340
S4.8	Steel	4.75	7490	5850	3190
S6	Steel	5.99	7710	5930	3245
S8	Steel	7.93	7693	5850	3350
G4	Glass	3.97	2552	5950	3300
G6.1	Glass	6.10	2653	5750	3410
G8	Glass	7.98	2477	5700	3410

[a]Data acquired from Ref. 36.

2. Experimental setup

The schematic diagram of the experimental setup developed in this paper for measuring the ARF by the weighing method is shown in Fig. 1. A concave piezoceramic source (with an air backing) in the form of a spherical bowl with a focal length of 70 mm and a diameter of 100 mm was placed in a 300 × 300 × 300 mm tank with degassed water. The resonant frequency of the piezoceramic plate was 1.072 MHz, and the bandwidth was approximately 0.15 MHz. A thermometer was used to measure and control the consistency of the water temperature during the experiments. The source was rigidly mounted on a positioning system (VP9000; Velmex, Inc., Bloomfield, NY) that allowed it to be translated in three mutually perpendicular directions with a positioning accuracy of 2.5 μm. The orientation of the source was pre-aligned with the water surface to direct the axis of the generated beam vertically downwards. A continuous wave harmonic signal (at a selected frequency in the vicinity of the resonance frequency of the source) was fed from the generator (Agilent 33250A; Agilent Technologies, Santa Clara, CA) through an amplifier (210L; Electronics & Innovation, Ltd., Rochester, NY) to the source. An elastic spherical target (a bead) was positioned at some distance from the source on its acoustic beam axis in the center of a large-diameter plastic auxiliary ring. The sphere was fixed using a system of four stretched thin fishing lines (Berkley Nanofil, Pure Fishing, Inc., Columbia, SC). Because of the small diameter of the lines (35.7 μm) their influence on the acoustic field was negligible.[36] The fishing lines were stretched tightly enough to reduce the possibility of spatial shift and vibration of the bead. According to the measurements, the displacement of the sphere did not exceed 0.3 mm at the maximum value of the radiation force achieved, which gives an estimate of more than 1 N for the tension of the fishing lines. The plastic ring was attached to a rigid frame that encircled the water tank without touching its walls and transferred the force applied to the bead directly to the surface of an electronic balance (VI-3mg; Acculab USA, Central Islip, NY). This construction enables to measure the vertical component of the ARF acting on the scatterer. The levels of precision of the balance and the scale division were 4 mg and 1 mg, respectively. In order to suppress the influence of hydrodynamic flows (acoustic streaming) induced by the ultrasound beam, a thin polyethylene film (food wrap with a thickness of less than 10 μm) was stretched over the scatterer at a distance of about 1 cm, acting as a thin sound-transparent membrane. The low membrane thickness ensured that the ultrasound beam was not absorbed or modified as it passed through. An acoustic absorber (HAM-A; Precision Acoustics, Dorchester, UK) was placed at the bottom of the tank to eliminate wave reflection from the bottom of the tank. The influence of reflections from the side walls was negligible, which was verified by comparing force measurements at different transverse positions of the transducer and the target. (The results were the same.) The signal at the source was measured by means of an oscilloscope (TDS5034B; Tektronix, Beaverton, OR).

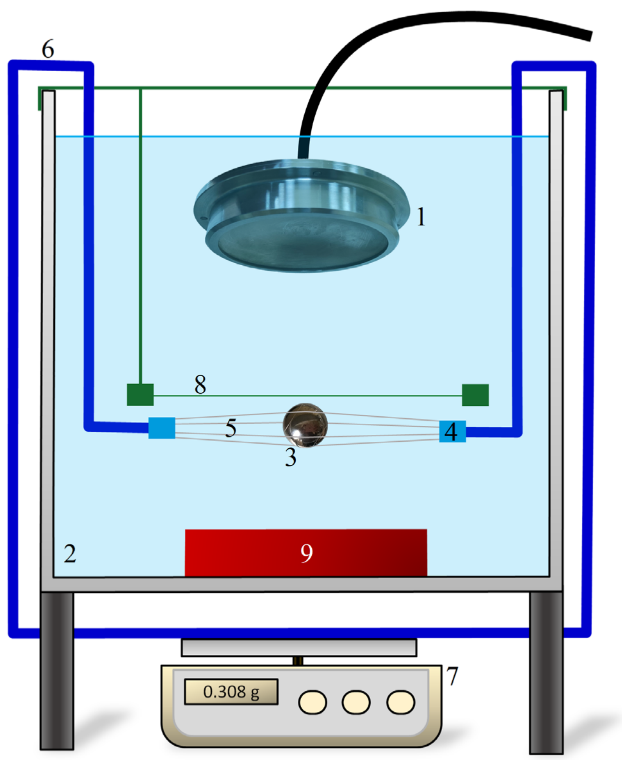

FIG. 1. Diagram of the experimental setup for measuring the ARF on an elastic sphere in water. (1) Source (fixed in a positioning system), (2) water tank, (3) spherical target, (4) ring construction for mounting the scatterer, (5) fishing lines, (6) a rigid frame resting on a balance, (7) electronic balance, (8) anti-streaming membrane, (9) absorber.

https://doi.org/10.1121/10.0035939

3. Techniques for ARF measurement and processing

To find the reference position of the sphere (position at the beam focus), a pulsed mode of operation was used. By moving the transducer both vertically and transversely, the amplitude of the pulsed signal reflected from the sphere surface back to the transducer (echo signal) was observed on an oscilloscope. The position of the sphere at the source focus was found by searching for the maximum of the reflected signal amplitude. To ensure the sphere was in focus, the delay time of the reflected signal was measured and compared with the calculated delay time $t_{delay} = 2(F - d/2)/c$, where F is the focal length of the source, d is the sphere diameter, and c is the speed of sound in water. The rates of accuracy of finding the focus were 0.7 mm along the vertical axis (equal to half a wavelength, caused by the uncertainty in determining the start of the acoustic signal from which the delay time is measured) and about 0.05 mm along the transverse axes (determined by the ability to detect on the oscilloscope the deviation of the amplitude of the pulse reflected from the sphere from its maximum value, which indicates that the sphere is off-axis).

The ARF measurements were carried out with the transducer in different positions in relation to the sphere. To measure the force on the beam axis, the transducer was moved along the vertical axis z in increments of 0.25 mm or 0.1 mm (for detailed results in the focal area).

In order to rule out the possibility of the sphere being accidentally displaced in the fishing lines by radiation force during measurements (which alters the coordinate of the sphere) or its falling out of the lines, a strong signal was applied to the transducer prior to ARF measurements, when the sphere was placed in the focus, generating a force slightly greater than the maximum force measured in experiments. This ensured that the sphere was securely and steadily fixed in fishing lines during further measurements.

The magnitude of the ARF was determined by the difference between the balance readings (m_{rad}) before and after the electrical signal was applied from the generator to the source. The formula

$$Y_z^{\exp} = \frac{m_{rad}\, g c}{W} \tag{9}$$

was used to convert the weighting result m_{rad} into a dimensionless ARF, $Y_z^{\exp}$. Here, $g = 9.81$ m/s^2 is the gravitational acceleration, $c = 1480$ m/s is the speed of sound in water, and W is the total acoustic beam power, calculated using Eq. (8).

For the experimental data processing and numerical calculations, MATLAB (MathWorks, Natick, MA) was used.

4. Measuring the field of the focused transducer

To calculate the ARF numerically, it is necessary to know the pressure angular spectrum of the source used in experiments. A transient acoustic hologram of the source was measured to determine the angular spectrum of the field incident on a sphere.[32] Here is a brief description of the method used. A pulsed electric voltage signal in the form of a tone burst, consisting of 5 cycles of a 1.072 MHz sinusoid with an amplitude of 5 V, was applied to the transducer from the generator. The acoustic signals of the radiated field were measured with a needle-type hydrophone (HNA-0400; Onda, Sunnyvale, CA) with a sensor diameter of 0.4 mm. The hydrophone was moved along three perpendicular axes (positioning accuracy $5\,\mu$m) by means of a computer-controlled positioning system (UMS-3; Precision Acoustics, Dorchester, UK). An acoustic hologram was recorded at a distance of $z_H = 55$ mm from the center of the source in the plane perpendicular to the beam axis. During the measurements, the hydrophone was moved with a spatial step of 0.5 mm between the points of the square grid (x, y) 201×201. (The aperture of the hologram was 100 mm.) An electric voltage signal in the time domain was recorded at each grid point. Fast Fourier transform was used to find the frequency spectrum of the time signal at each point of the hologram (x, y). Next, the complex amplitude of the electric voltage at the frequency of interest, $\omega_0 = 2\pi f_0$, was extracted from the spectrum. This value was normalized to the complex amplitude of the electrical signal at the source, at the same frequency, ω_0. The value obtained, $U(x, y, \omega = \omega_0)$, describes the distribution of the complex amplitude in the measurement plane corresponding to the monochromatic mode of the source at the frequency ω_0 with a voltage amplitude of 1 V. The spatial spectrum of the signal was then calculated using the formula

$$S_U(k_x, k_y, \omega_0) = \int_{-\infty}^{+\infty}\int_{-\infty}^{+\infty} dxdy U(x, y, \omega_0) e^{-ik_x x - ik_y y}. \tag{10}$$

This spectrum was further corrected for known hydrophone directivity, $D(k_x, k_y, \omega_0)$, and sensitivity, $M_0(\omega_0)$:[32]

$$S_{corr}(k_x, k_y, \omega_0) = \frac{S_U(k_x, k_y, \omega_0)}{M_0(\omega_0) D(k_x, k_y, \omega_0)}. \tag{11}$$

To obtain the true pressure angular spectrum, $S(k_x, k_y, \omega_0)$, for ARF calculations, the corrected spatial spectrum, S_{corr}, was multiplied by the value of the complex amplitude of the electrical signal, $U_{tr}(\omega_0)$, applied to the transducer during ARF measurements:

$$S(k_x, k_y, \omega_0) = U_{tr}(\omega_0) S_{corr}(k_x, k_y, \omega_0). \tag{12}$$

The true structure of the field produced by the source can be reconstructed from this spectrum:

$$p(x, y, z, \omega_0) = \frac{1}{4\pi^2} \int\int_{-\infty}^{+\infty} dk_x dk_y S(k_x, k_y, \omega_0) \times e^{ik_x x + ik_y y + i\sqrt{k^2 - k_x^2 - k_y^2}(z - z_H)}. \tag{13}$$

The pressure angular spectrum $S(k_x, k_y, \omega_0)$ calculated from the hologram can be used to calculate the ARF at different sphere positions in the beam.[14] The expression for the angular spectrum when the sphere is located at the point with the coordinates (x_s, y_s, z_s) relative to the position $(0, 0, z_H)$, corresponding to the position of the measured hologram, is as follows:

$$S(k_x, k_y, \omega_0)|_{(x_s,y_s,z_s)} = S(k_x, k_y, \omega_0)|_{(0,0,z_H)} e^{ik_x x_s + ik_y y_s + i\sqrt{k^2-k_x^2-k_y^2}(z_s-z_H)}. \quad (14)$$

5. Control of the wave reflection from the transducer

An empirical study was carried out to analyze the coefficient of sound reflection from a piezoceramic transducer as a function of frequency and active impedance of the electrical load of the transducer, following a similar experimental technique described in Ref. 35.

The experimental setup is similar to that used for ARF measurements. An elastic sphere was located at the focus of the PT. A sinusoidal signal of 5 V amplitude consisting of 5 periods at the antiresonance frequency was applied to the source. The PT emitted an acoustic wave that propagated towards the sphere, reflected from it, and returned to the PT. After reflection from the PT, the wave propagated back to the sphere and reflected from it once more. An oscilloscope was used to record electrical signals on the PT: reflected and re-reflected waves. The ratio of amplitudes of frequency spectra of these waves, R_{refl}^{eff}, is proportional to the reflection coefficient from the PT and also takes into account wave reflection losses from the sphere material and diffraction losses associated with the divergence of the wave.[35] For the purposes of this work, it is not necessary to know the exact values of losses, as we look for parameters (frequency and electrical load resistance) that ensure the minimum reflection from the PT, taking into account all the losses (also present in ARF measurements). Therefore, the experimental quantity of interest is the magnitude of the value R_{refl}^{eff}, which is henceforth referred to as the coefficient of effective reflection from the PT.

The internal resistance of the generator was 50 Ω and acted as an electrical impedance loaded on the conducting sides of the piezoelectric plate when operating in the receive mode. Different resistances were additionally connected in series or parallel to the generator to obtain different values of the total electrical impedance Z_{el} loaded on the piezoelectric transducer. To ensure a minimum inductive component, 10, 51, and 100 Ω precision resistors (metal film resistors, MF-25 (C2–23) 0.25 W, 1% accuracy; Synton-Tech, Taiwan) were used. By connecting them in series and parallel in various combinations, different resistance values were obtained.

According to theory, the minimum reflection coefficient from the PT should be expected at the connected electrical load with an impedance equal to the complex conjugate of the PT impedance (which is real at the antiresonance frequency). The deviation from this value will be the greater the more the operation of a real PT differs from that of the ideal theoretical model,[35] and the load impedance will also be affected by the presence of electrical and mechanical losses in the piezoceramics, diffraction losses due to the finite size of the piezoelectric plate and the setup, inhomogeneity of the piezoelectric plate, etc.

III. RESULTS AND DISCUSSION

A. Holographic reconstruction of the acoustic beam structure

Figure 2 illustrates the measured magnitude and phase of the acoustic pressure field $p(x, y, \omega_0)$ in the acoustic hologram plane at the frequency of $f_0 = \omega_0/2\pi = 1.072$ MHz (top row), the magnitude and phase of the angular spectrum (middle row) calculated for this field, and the field of the source in the axial plane, calculated by Eq. (13) (bottom). As expected, the field structure of the source is not strictly axisymmetric, as would be the case for an ideal piston radiator, so measuring the acoustic hologram is essential for accurate ARF calculation.

B. Numerical calculation of ARF

Equations (1)–(8) were used to calculate the ARF on an elastic sphere for the acoustic beam used in the presented experiments, with the angular spectrum determined from hologram measurements. The number of terms in the infinite series in Eq. (1) was $N_{max} = (3\text{–}5)ka$, which was sufficient for convergence.[37] Figure 3 shows the results of calculations of two-dimensional distributions of the axial force component for the scatterers S6 and G6.1 in the (x, z) plane. It can be seen that the maximum value of the force is reached in the focal region, and its magnitude decreases rapidly with distance from the focus. The ARF distribution for S6 is smoothly decreasing in the pre-focal region, while the sphere G6.1 has a non-uniform force distribution; i.e., a dependence on the azimuthal angle appears. During the experiments, the force was measured along the acoustic beam axis (along the z axis at $x = 0$, $y = 0$).

C. Selection of the electrical load of the transducer to suppress the reflection coefficient from its surface

The frequency dependence of the impedance of the piezoelectric transducer was measured, and the antiresonance frequency 1.072 MHz and the real part of the impedance at this frequency 13 Ω (the imaginary part becomes zero) were determined from these data.

For spheres larger than 6 mm in diameter, the effective reflection coefficient from the PT R_{refl}^{eff} was measured. The value of the electrical load of the transducer Z_{el} was varied from 2 to 100 Ω in steps of 1.3 to 20 Ω (17 different values in total), depending on the theoretically assumed rate of change of the reflection coefficient [see Eq. (4) in Ref. 35].

The left graph in Fig. 4 shows the experimentally obtained distribution of $|R_{refl}^{eff}|$ as a function of frequency f and the value of the resistance of the electrical load R using sphere S6 as a scatterer. The experimental plot is smoothed for clarity. The right graph in Fig. 4 shows the same value $|R_{refl}^{eff}|$ for three representative frequencies as a function of

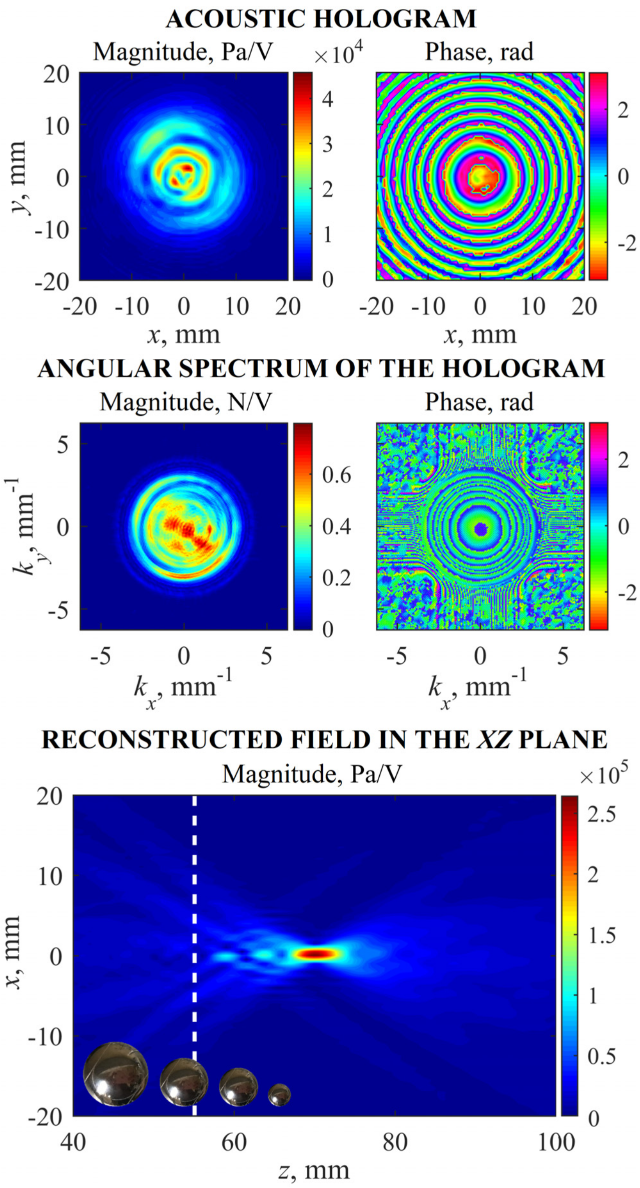

FIG. 2. (Top) Transverse distribution of the magnitude and phase of the pressure field at a frequency of 1.072 MHz from acoustic hologram measured at a distance $z_H = 55$ mm. (Middle) Magnitude and phase of the corresponding angular spectrum. (Bottom) Distribution of the acoustic pressure magnitude in the axial plane in water, reconstructed from the acoustic hologram. The pressure magnitude is normalized by the corresponding magnitude of the voltage applied to the transducer. The white vertical dashed line depicts the plane of the hologram measurement. Spheres used in ARF experiments (S8, S6, S4.8, S2.8) are shown to scale.

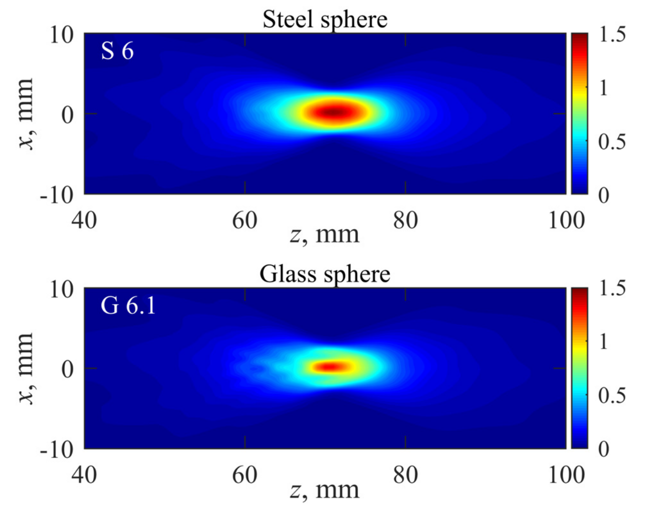

FIG. 3. Spatial distributions of the axial component of the dimensionless acoustic radiation force Y_z for steel S6 (top) and glass G6.1 (bottom) spheres positioned at any point in the xz plane at $y = 0$.

the electrical load resistance R. The minimum value of $|R^{eff}_{refl}| = 0.017$ is achieved at 1.071 MHz with a 20 Ω electrical load of the PT. (The load is obtained by connecting a combination of resistors with a total resistance of 33 Ω in parallel with a generator with an internal resistance of 50 Ω.) Consequently, by applying the same electrical load during ARF measurements, it is possible to reduce the coefficient of reflection from the transducer of the waves scattered by the sphere located at the focus and to minimize the influence of standing waves on the force measurement results.

Similar measurements were conducted with glass (G6.1, G8) and steel (S8) spheres. The load and frequency values at which the effective reflection coefficient is minimal were found to vary slightly between different spheres (1.074 MHz and 20 Ω for S8, 1.074 MHz and 25 Ω for G6.1, 1.072 MHz and 20 Ω for G8). This discrepancy can be attributed to the fact that the initial assumption made in the theory, namely that a spherical wave is incident upon a spherical transducer, is only approximately fulfilled. First, the wave scattered on an elastic sphere will have an inhomogeneous angular distribution of the scattered field structure (which will vary for different sphere diameters and materials),[38] second, the acoustic beam that falls on the sphere is not perfectly axisymmetric and does not have an ideal spherical front. Thus, in a real situation, the assumption of spherical character of the reflected wave is violated, different parts of the piezoelectric plate vibrate differently, and the theoretical effect of complete reflection cancellation is not achieved. Furthermore, the structure of the scattered wave incident on the transducer changes significantly when the sphere is positioned at different points in the field. A distance of 1 mm from the focus reveals a marked divergence from the spherical wave front [proved by calculations carried out according to the Eq. (8) from Ref. 36]. It can thus be concluded that the suppression of the reflection coefficient from the PT at the aforementioned parameters (load resistance and frequency) will be realized only in a small vicinity of the focus.

D. ARF measurements

ARF measurements were performed for the spheres listed in Table I. The parameters used for each sphere are listed in Table II. In most cases, ARF measurements were performed at the center frequency of the transducer (1.072 MHz). In certain cases, frequencies close to the center frequency were used due to the prior selection of

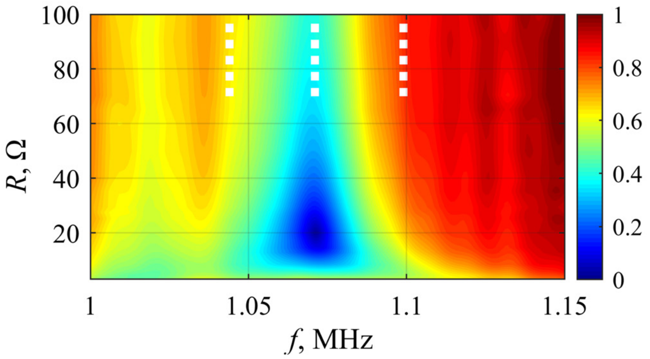

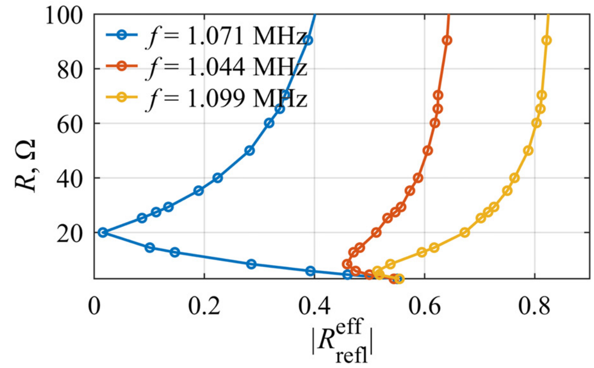

FIG. 4. (Left) Magnitude of the coefficient of effective reflection from the focused piezoelectric transducer $|R_{refl}^{eff}|$ as a function of the frequency f and the value of the active load of the transducer R with a steel sphere, S6, positioned in focus and used as a reflector. The white dashed lines indicate the frequencies at which this distribution is shown in the right graph. (Right) Magnitude of the coefficient of effective reflection $|R_{refl}^{eff}|$ as a function of the value of the active load of the transducer R at different frequencies: A frequency of 1.071 MHz provides a minimum reflection coefficient $|R_{refl}^{eff}| = 0.017$ at a 20 Ω load. The circles represent the values of the active loads realized in the experiment.

parameters (frequency and load resistance) that would minimize the reflection from the piezotransducer (see Sec. III C). In this case, measurements were carried out both with and without the additional PT load at the same selected frequency. (The resistance of the resistor to be connected in parallel to the generator is given in Table II.)

The water temperature did not change during a single set of measurements, which usually lasted several hours and ranged from 21 to 23 °C for different sets. The source voltage was selected to ensure that the uncertainties in the measured force (because of the balance error 4 mg) at the beam focus would be less than 1%, with the absolute balance error, $\Delta Y_z^{(balance)}$, at all points being less than 0.02. The balance readings during the ARF measurements ranged from 10 mg (0.1 mN) for ARF far from the focus to 200–650 mg (2–6.5 mN) at the beam focus, while the acoustic power ranged from 3.1 to 6.2 W.

Figure 5 shows a typical time dependence of the scale readings during an ARF measurement. The record is made when the balance is connected to a computer. First, before the generator was switched on, the scale readings were recorded. After switching on the generator, a short period of time (usually less than 2 s) was required to establish a constant force value (which was also recorded) and to dampen any possible oscillations of the bead within the fishing lines excited by the impact of the incident beam. The end of the oscillation damping could also be observed by the establishment of a stable signal amplitude on the oscilloscope. The difference (m_{rad}) between the two force values was then converted to the dimensionless radiation force $Y_z^{\exp}$ by means of Eq. (9). After switching off the signal, the scale readings were compared with those before switching on. The cases of inequality indicated a sudden change in the external conditions during a single act of measurement (e.g., bubbles forming or floating on submerged structural elements) and the necessity for the repetition of measurement at this point. It has been verified that repeated ARF measurements at the same point (both in and out of focus area) give the same result to within 1 mg; i.e., repeatability of measurements under constant conditions was observed.

TABLE II. Parameters of the electrical part of the setup used during ARF measurements.

Sample	Frequency (MHz)	Source voltage (V)	Acoustic power W (W)	Additional PT load[a]
S2.8	1.072	9.02	3.10	—
S4.8	1.072	10.99	4.61	—
S6	1.071	10.87	3.58	—
		10.67	3.45	33 Ω
S8	1.074	9.04	3.12	—
		9.59	3.51	33 Ω
G4	1.072	12.74	6.20	—
G6.1	1.074	10.94	4.56	—
		11.67	5.19	51 Ω
G8	1.072	10.99	4.61	—
		10.71	4.38	33 Ω

[a]—, no additional load.

The results of experimental measurements of the vertical ARF component as a function of distance z along the acoustic beam axis are presented in Fig. 6 for steel spheres and in Fig. 7 for glass spheres of different diameters. The black dots in Figs. 6 and 7 represent the results of direct ARF measurements with a step along the z axis of 0.25 mm out of focus and 0.1 mm in focal area. These points were then connected by a continuous smooth curve using the "spline" function (in MATLAB). Yellow curves correspond to experimental results for ARF measurement without additional PT load (without compensation for sound reflection from PT). The black curves are calculated numerically.

In the focal region, significant discrepancies with the theoretical curves are observed. Oscillations of 30%–60% amplitude (relative to the average level) appear, associated with the occurrence of standing waves between the transducer and the scatterer surfaces. In this case, the oscillation period should be equal to half the wavelength, i.e., approximately 0.7 mm. This period can be resolved by the step size used (0.1–0.25 mm).

In regions where the conditions for standing wave generation are not well fulfilled (out-of-focus regions where the

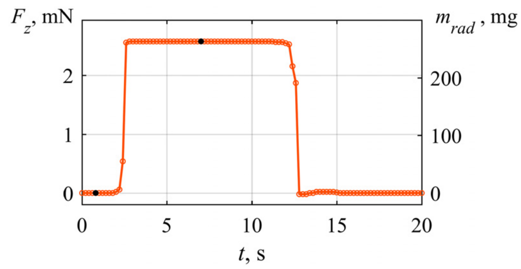

FIG. 5. Typical time dependence of balance readings during ARF measurements. The black dots before and after turning on the generator indicate the values used to calculate the force m_{rad}. The error $\Delta Y_z^{(balance)}$ (related to the balance accuracy) is comparable to the size of the circles that correspond to the measurement points.

wavefront of the incident wave does not coincide with the sphere surface), the influence of oscillations is much smaller and their amplitude is comparable to the measurement error (40 μN).

1. Comparison of experimental results with theory

Measurement results were compared with numerical calculations of ARF. As can be seen from Figs. 6 and 7, the theoretical (black) curves overlap well with the experimental curves on average.

Sometimes the theoretical curves in the prefocal region slightly exceed the experimentally measured values, which may be due to the small inclination of the source from the vertical orientation, resulting in a tilt of the axis along which the measurements were made relative to the acoustic beam axis. For measurements with different spheres, this tilt was estimated by finding the central point (with maximum force) of the transverse force distribution in the plane perpendicular to the vertical axis, before and after the focus, where the force oscillations were small. The tilt angle for all measurements was about 5°–8°. This slight tilt is due to the way the transducer is mounted and the challenge of aligning it more accurately. Another source of errors of the same type is the misalignment of the normal to the hologram with the direction of the acoustic axis of the source. The impact of the tilt between the calculation and measurement axes on the calculation of the dimensionless ARF was investigated. The maximum observed error was $\Delta Y_z^{tilt} = 0.1$ (marked in the plot for S4.8 in Fig. 6). This error can explain the small discrepancy between the experimental and theoretical force values in the pre-focal region. Taking into account the ARF inhomogeneity in the pre-focal region (dependence of the force on the azimuthal angle), the influence of tilt on the force measurements will be more pronounced for glass spheres compared to steel spheres (see Fig. 3). For a steel sphere, S6, the theoretical curve in Fig. 6 is calculated for a line inclined at 8° to the z axis.[27] It is therefore possible to slightly improve the agreement between experiment and theory by varying the axis tilt in calculations or by more accurate positioning and orientation of the transducer in space.

2. Averaging of the experimental data

For the steel spheres S2.8 and S4.8 (Fig. 6), the blue dashed lines show the results of averaging of the

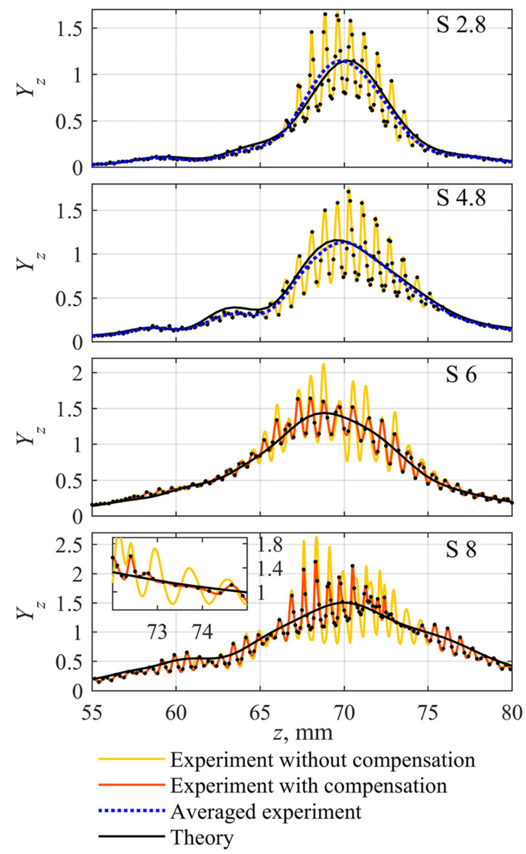

FIG. 6. Distributions of the vertical (axial) component of the dimensionless ARF Y_z along the beam axis z for steel spheres of different diameters. The sample names of the spheres used as the target are shown at the top right of each plot. The error of experimental measurements $\Delta Y_z^{(balance)}$ is comparable to the linewidth. The black dots represent the results of direct ARF measurements at each coordinate point.

experimental curves (averaging of the oscillations); i.e., the Fourier transform of the extrapolated experimental curve was performed and the high frequency spectrum responsible for the oscillations was zeroed (low pass filtering). The results of averaging are quite close to the theoretical curves. Nevertheless, the averaging procedure is not entirely correct, as it requires extrapolation of the data to the outer domain (beyond the z axis measurement limits), and the result of the averaging depends on the averaging parameters (on the selected cutoff frequency). In addition, the complex field structure between the transducer and the scatterer changes radically with a small displacement of the scatterer. This can affect the shape and amplitude of the force oscillations in unpredictable ways. Thus, averaging can only present the data in a more convenient form close to the real one, but it does not provide the true distribution of ARF on the axis in the absence of standing waves.

3. ARF measurement with an additional electrical load to suppress the reflection from the PT

In order to reduce the influence of standing waves on the results of the ARF measurements (and consequently to reduce the amplitude of the force oscillations on the z axis),

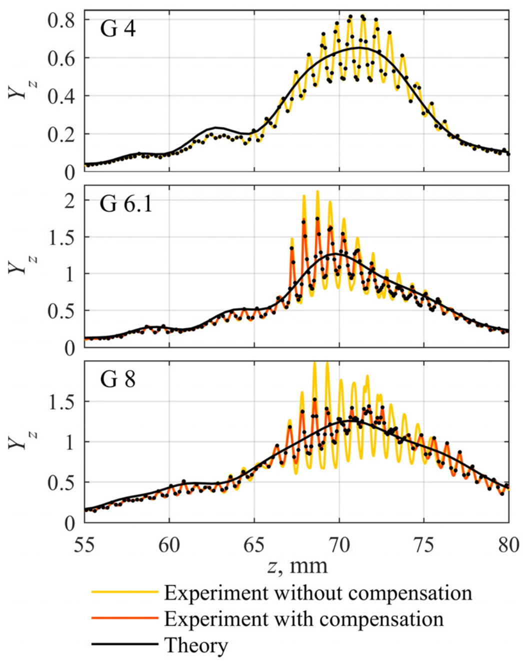

FIG. 7. Distributions of the vertical (axial) component of the dimensionless ARF Y_z along the beam axis z for glass spheres of different diameters. The sample names of the spheres are shown at the top left of each plot. The error of experimental measurements $\Delta Y_z^{(balance)}$ is comparable to the linewidth. The black dots represent the results of direct ARF measurements at each coordinate point.

the electrical part of the experimental setup was modified: A resistor of selected resistance (see Table II) was connected in parallel to the generator to reduce the reflection of acoustic waves from the PT surface. 33 and 51 Ω metal oxide film resistors (MOX Jantzen metallized, 5 W, 5%; Jantzen Audio, Praestoe, Denmark) were used.

In Figs. 6 and 7, the red curves correspond to the results of ARF measurement experiments with additional PT load (with compensation for sound reflection from PT). The use of an additional PT load reduced the amplitude of force oscillations by an average of 1.5–4 times. Furthermore, for the S8 and G8 spheres, the suppression becomes particularly noticeable near certain points: at the focal point (70 mm) and behind the focal point (73–74 mm). It can be reasonably assumed that at these points, the sphericity conditions for the wave incident on the PT are best fulfilled. At the bottom graph in Fig. 6, there is an inset with an enlarged section of the graph showing the region where the suppression of oscillations proved to be almost complete. In general, due to the complex inhomogeneous structure of the beam incident on the scatterer and the scattered field, the suppression of standing waves (selection of the electrical load) strongly depends on both the size/material of the sphere and its position in space relative to the transducer. Therefore, a selected resistor can help to reduce oscillations, but the extent of the reduction depends on the specific case.

Overall, despite the lack of complete suppression of standing waves generated between the surfaces of the scatterer and the PT, a significant reduction in the amplitude of oscillations was achieved in the focal region where standing waves are most effectively formed. Consequently, the method of reducing the coefficient of reflection from the transducer, associated with the selection of its electrical load,[35] can be used to some approximation for the spherical piezoelectric transducer as well.

4. Experimental linearity of the ARF with acoustic power

According to theory [see Eqs. (1)–(8)], the radiation force ($F_z = m_{rad}\, g$) is linearly proportional to the total acoustic beam power W. Deviations from the linear dependence may indicate, for example, the presence of nonlinear effects in the acoustic beam propagation, hydrodynamic flows, cavitation or incorrect operation of the setup. To verify this, the dependence of the vertical ARF component F_z on the magnitude of the total acoustic beam power was measured. Figure 8 shows the results of the ARF measurements at four different points on the acoustic axis of the beam together with the dashed lines obtained using least squares method (LSM). In the region behind the focus (point coordinates 76.0 and 78.0 mm), where the force oscillations due to standing waves are weak, a good linear dependence was observed for the whole power range investigated. Both lines obtained with LSM (black and blue dashed lines on the graph) have a very good correlation of $R^2 = 0.999$. Force measurements in front of the focus showed similar results. Force measurements in the focal region (point coordinates 69.8 and 70.1 mm) showed a linear dependence on total acoustic power only at low power levels (up to 3–6 W, depending on the coordinate and the sphere used). As the power was increased, small deviations from linearity were observed, both up (70.1 mm) and down (69.8 mm), depending on the coordinate of the sphere position. Studies have shown that these deviations are caused by the displacement of the sphere together with the fishing lines under the action of the ARF (greater than about 1.5 mN) to the point where the ARF value, due to standing waves, differs from the ARF value at the initial point. Depending on whether the force at this point is greater or less, deviations from linearity are observed in the greater or lesser direction, respectively. Taking into account the presence of strong oscillations of the force in the focal area, it can be considered that this phenomenon does not have a discernible influence on the overall character of the force dependence measured along the axis. Therefore, in accordance with the theoretical model used, it can be concluded that the ARF is linear over the range of powers used.

To reduce the relative error of the balance, it is necessary to increase the power of the signal applied to the source, thereby increasing the magnitude of the ARF. However, the role of nonlinear effects (causing higher harmonics to appear) in wave propagation increases with increasing power. To assess the influence of higher harmonics, the frequency spectrum of the acoustic field in the focal area was examined. The acoustic signals were measured by a needle-type hydrophone (Onda HNA-0400; Onda, Sunnyvale, CA). It was found that for the maximum voltage at the source used in experiments, the second harmonic

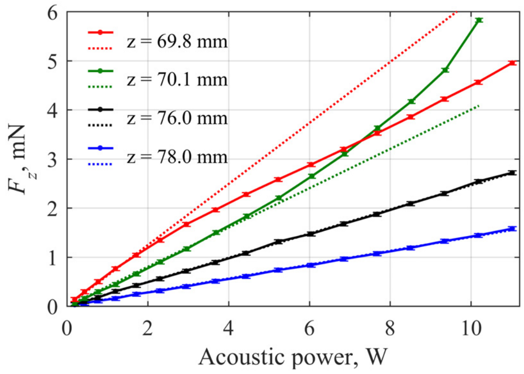

FIG. 8. Dependence of the ARF F_z on the total acoustic beam power W. The results are presented for different points on the beam axis. Coordinate points 76.0 mm and 78.0 mm correspond to the region behind the focus. Coordinate points 69.8 and 70.1 mm correspond to the focal area. The dots indicate the results of experimental measurements. Error bars show the error of the experimental measurements $\Delta F_z^{(balance)}$. Dashed lines are obtained using the least squares method (LSM). For measurements behind the focus (76.0, 78.0 mm), the LSM is applied to all points. For points from the focal region, the LSM is applied to points corresponding to low power levels.

amplitude at the focus does not exceed 24% of the first harmonic amplitude, and it is less than 12% (2%) at a distance of 10 mm behind (before) the focus. Since the ARF is quadratic to the amplitude of the incident wave, the contribution of the second harmonic to the ARF is less than 6% at the focus and less than 1.5% at a distance of 10 mm. Since the higher harmonics are effectively generated only at the beam focus, the beam width of the second harmonic is much smaller than the first harmonic beam width, which also reduces the expected magnitude of the ARF of the second harmonic. Thus, for the source voltages used, the generation of higher harmonics is negligible and does not affect the ARF value.

5. Acoustic streaming

In addition to acting on the scatterer, the acoustic wave can act directly on the propagation medium. High-intensity acoustic waves in liquids (and gases) produce directional motion of the medium itself, called acoustic streaming.[39] Acoustic streaming can affect the measured force in unpredictable ways, so a sound-transparent anti-streaming membrane was placed directly above the scatterer.

The effect of the membrane on the force measured was investigated. It was found that the presence of the membrane and the change in its position relative to the sphere did not affect the magnitude of the force (the difference is within the error of the balance) and its invariance over time. Hence, for a given experimental setup configuration, measurement time, and power levels used, acoustic streaming values are weak or absent and the use of a membrane is not essential. Nevertheless, the membrane was left to exclude cavitation regimes, as well as cases where bubble nuclei adhere to the surface of the sphere (these bubbles would later float to the membrane surface).

6. Comparison of identical targets

To demonstrate the reliability of the method, additional experiments were also performed for identical scatterers (of the same material and diameter). The curves obtained for different identical spheres (G4 and S4.8) overlapped well, providing indirect evidence of the reproducibility of the experimental results. This also indicates a good equivalence of the scatterers used, in particular the homogeneity of their internal structure.

IV. CONCLUSIONS

In this study, a precise method is described for measuring the axial component of the acoustic radiation force of an acoustic beam of arbitrary shape acting on an elastic sphere of millimeter diameter placed on the beam axis. The force value is determined from the results of the weighing, similar to the radiation force balance method of measuring the total power of an acoustic beam incident on an extended absorber. The results obtained have demonstrated the validity and the reliability of the proposed method. An accuracy of 40 μN was achieved with the electronic scales used. In the axial distribution of the measured radiation force, strong oscillations were observed in the focal region due to the generation of standing waves between the surface of the piezoelectric transducer and the target. It is shown that at a certain electrical load (active load when considering the vicinity of the antiresonance frequency) of the piezoelectric transducer, the reflection coefficient from the transducer decreases, reducing the amplitude of the force oscillations by an average of 1.5–4 times near the focus and improving the accuracy of the radiation force measurements. Experimental results are compared with numerical calculations using the SB model based on angular spectrum decomposition. For different sphere diameters and materials, overall agreement is shown.

ACKNOWLEDGMENTS

This work was supported by a student stipend from the “BASIS” Foundation (Foundation for the Advancement of Theoretical Physics and Mathematics Grant No. 22-2-10-14-1 to L.M.K.). The authors would like to thank Dr. Michael Bailey for valuable discussions.

AUTHOR DECLARATIONS

Conflict of Interest

The authors have no conflicts to disclose.

Ethics Approval

The presented study did not involve animals and/or human subjects.

DATA AVAILABILITY

The data that support the findings of this study are available within the article.

[1]A. P. Sarvazyan, O. V. Rudenko, and W. L. Nyborg, "Biomedical applications of radiation force of ultrasound: Historical roots and physical basis," Ultrasound Med. Biol. **36**(9), 1379–1394 (2010).
[2]A. Ozcelik, J. Rufo, F. Guo, Y. Gu, P. Li, J. Lata, and T. J. Huang, "Acoustic tweezers for the life sciences," Nat. Methods **15**(12), 1021–1028 (2018).
[3]S. Inoue, S. Mogami, T. Ichiyama, A. Noda, Y. Makino, and H. Shinoda, "Acoustical boundary hologram for macroscopic rigid-body levitation," J. Acoust. Soc. Am. **145**(1), 328–337 (2019).
[4]A. P. Sarvazyan, O. V. Rudenko, and M. Fatemi, "Acoustic radiation force: A review of four mechanisms for biomedical applications," IEEE Trans. Ultrason, Ferroelect, Freq. Contr. **68**(11), 3261–3269 (2021).
[5]A. Krokhmal, O. Sapozhnikov, E. Koudan, S. Tsysar, Y. Khesuani, and V. Parfenov, "Assembly of a ring-shaped construct from tissue spheroids in a magneto-acoustic field," Proc. Mtgs. Acoust. **38**(1), 020006 (2019).
[6]T. T. Chen, P. C. Samson, M. D. Sorensen, and M. R. Bailey, "Burst wave lithotripsy and acoustic manipulation of stones," Curr. Opin. Urol. **30**(2), 149–156 (2020).
[7]M. D. Sorensen, B. Dunmire, J. Thiel, B. W. Cunitz, B. Burke, B. J. Levchak, C. Popchoi, A. R. Holmes, M. K. Hall, M. Dighe, Z. Liu, M. R. Bailey, M. Porter, and J. D. Harper, "Randomized controlled trial of ultrasonic propulsion-facilitated clearance of residual kidney stone fragments vs observation," J. Urol. **212**(6), 811–820 (2024).
[8]M. A. Ghanem, A. D. Maxwell, Y.-N. Wang, B. W. Cunitz, V. A. Khokhlova, O. A. Sapozhnikov, and M. R. Bailey, "Noninvasive acoustic manipulation of objects in a living body," Proc. Natl. Acad. Sci. U.S.A. **117**(29), 16848–16855 (2020).
[9]P. C. May, M. R. Bailey, and J. D. Harper, "Ultrasonic propulsion of kidney stones," Curr. Opin. Urol. **26**(3), 264–270 (2016).
[10]Y. P. Qiao, M. Gong, H. Wang, J. Lan, T. Liu, J. Liu, Y. Mao, A. He, and X. Liu, "Acoustic radiation force on a free elastic sphere in a viscous fluid: Theory and experiments," Phys. Fluids **33**(4), 047107 (2021).
[11]T. S. Jerome, Y. A. Ilinskii, E. A. Zabolotskaya, and M. F. Hamilton, "Acoustic radiation force on a compressible spheroid," J. Acoust. Soc. Am. **148**(4), 2403–2415 (2020).
[12]Y. A. Ilinskii, E. A. Zabolotskaya, B. C. Treweek, and M. F. Hamilton, "Acoustic radiation force on an elastic sphere in a soft elastic medium," J. Acoust. Soc. Am. **144**(2), 568–576 (2018).
[13]T. S. Jerome and M. F. Hamilton, "Born approximation of acoustic radiation force and torque on inhomogeneous objects," J. Acoust. Soc. Am. **150**(5), 3417–3427 (2021).
[14]O. A. Sapozhnikov and M. R. Bailey, "Radiation force of an arbitrary acoustic beam on an elastic sphere in a fluid," J. Acoust. Soc. Am. **133**(2), 661–676 (2013).
[15]D. Baresch, J.-L. Thomas, and R. Marchiano, "Three-dimensional acoustic radiation force on an arbitrarily located elastic sphere," J. Acoust. Soc. Am. **133**(1), 25–36 (2013).
[16]Z. Gong and M. Baudoin, "Equivalence between angular spectrum-based and multipole expansion-based formulas of the acoustic radiation force and torque," J. Acoust. Soc. Am. **149**(5), 3469–3482 (2021).
[17]T. F. W. Embleton, "Mean force on a sphere in a spherical sound field. II. (Experimental)," J. Acoust. Soc. Am. **26**(1), 46–50 (1954).
[18]T. Hasegawa and K. Yosioka, "Acoustic radiation force on fused silica spheres, and intensity determination," J. Acoust. Soc. Am. **58**(3), 581–585 (1975).
[19]F. Dunn, A. J. Averbuch, and W. D. O'Brien, "A primary method for the determination of ultrasonic intensity with the elastic sphere radiometer," Acta Acust. United Acust. **38**(1), 58–61 (1977).
[20]S. Chen, G. T. Silva, R. R. Kinnick, J. F. Greenleaf, and M. Fatemi, "Measurement of dynamic and static radiation force on a sphere," Phys. Rev. E **71**(5), 056618 (2005).
[21]A. V. Nikolaeva, S. A. Tsysar, and O. A. Sapozhnikov, "Measuring the radiation force of megahertz ultrasound acting on a solid spherical scatterer," Acoust. Phys. **62**(1), 38–45 (2016).
[22]B. E. Simon and M. F. Hamilton, "Measurement of acoustic radiation force on a sphere near a boundary," Proc. Mtgs. Acoust. **51**(1), 045002 (2023).
[23]M. A. Ghanem, A. D. Maxwell, O. A. Sapozhnikov, V. A. Khokhlova, and M. R. Bailey, "Quantification of acoustic radiation forces on solid objects in fluid," Phys. Rev. Appl. **12**(4), 044076 (2019).
[24]M. Karzova, A. Nikolaeva, S. Tsysar, V. Khokhlova, and O. Sapozhnikov, "Measurement and modeling of acoustic radiation force of focused ultrasound beam on an elastic sphere in water," Proc. Mtgs. Acoust. **32**(1), 045011 (2017).
[25]A. Nikolaeva, M. Karzova, S. Tsysar, V. Khokhlova, and O. Sapozhnikov, "Experimental study of radiation force by a focused ultrasound beam on an elastic scatterer in a fluid," Proc. Mtgs. Acoust. **38**(1), 045009 (2019).
[26]S. Vincent, P. Challande, and R. Marchiano, "Calibration of the axial stiffness of a single-beam acoustic tweezers," Rev. Sci. Instrum. **94**(9), 095102 (2023).
[27]O. Sapozhnikov, L. M. Kotelnikova, D. A. Nikolaev, and S. A. Tsysar, "Direct measurement of the radiation force of a focused acoustic beam on a spherical particle in water," Proc. Mtgs. Acoust. **48**(1), 045005 (2022).
[28]S. Tsysar, W. Kreider, and O. Sapozhnikov, "Improved hydrophone calibration by combining acoustic holography with the radiation force balance measurements," Proc. Mtgs. Acoust. **19**(1), 055015 (2013).
[29]D. Cathignol and O. A. Sapozhnikov, "On the application of the Rayleigh integral to the calculation of the field of a concave focusing radiator," Acoust. Phys. **45**(6), 735–742 (1999).
[30]O. A. Sapozhnikov and M. A. Smagin, "Finding the dispersion relations for Lamb-type waves in a concave piezoelectric plate by optical visualization of the ultrasound field radiated into a fluid," Acoust. Phys. **61**(2), 181–187 (2015).
[31]O. A. Sapozhnikov, S. A. Tsysar, V. A. Khokhlova, and W. Kreider, "Acoustic holography as a metrological tool for characterizing medical ultrasound sources and fields," J. Acoust. Soc. Am. **138**(3), 1515–1532 (2015).
[32]D. A. Nikolaev, S. A. Tsysar, V. A. Khokhlova, W. Kreider, and O. A. Sapozhnikov, "Holographic extraction of plane waves from an ultrasound beam for acoustic characterization of an absorbing layer of finite dimensions," J. Acoust. Soc. Am. **149**(1), 386–404 (2021).
[33]B. Issenmann, R. Wunenburger, S. Manneville, and J.-P. Delville, "Bistability of a compliant cavity induced by acoustic radiation pressure," Phys. Rev. Lett. **97**(7), 074502 (2006).
[34]P. Lidon, L. Villa, N. Taberlet, and S. Manneville, "Measurement of the acoustic radiation force on a sphere embedded in a soft solid," Appl. Phys. Lett. **110**(4), 044103 (2017).
[35]L. M. Kotelnikova, A. A. Krokhmal, D. A. Nikolaev, S. A. Tsysar, and O. A. Sapozhnikov, "Controlling the coefficient of reflection of sound from a plane piezoelectric plate by selecting its electrical load," Bull. Russ. Acad. Sci. Phys. **85**(12), 1501–1506 (2021).
[36]L. M. Kotelnikova, D. A. Nikolaev, S. A. Tsysar, and O. A. Sapozhnikov, "Determination of the elastic properties of a solid sphere based on the results of acoustic beam scattering," Acoust. Phys. **67**(4), 360–374 (2021).
[37]W. J. Wiscombe, "Improved Mie scattering algorithms," Appl. Opt. **19**(9), 1505–1509 (1980).
[38]J. J. Faran, "Sound scattering by solid cylinders and spheres," J. Acoust. Soc. Am. **23**(4), 405–418 (1951).
[39]O. V. Rudenko, "Three nonlinearities in physics of acoustic flows," Dokl. Phys. **65**(9), 317–322 (2020).